Diagnostic of manufacturing defects in ultrasonically welded thermoplastic composite joints using ultrasonic guided waves

Ochôa, Pedro; Villegas, Irene Fernandez; Groves, Roger M.; Benedictus, Rinze

DOI
10.1016/j.ndteint.2019.102126

Publication date
2019

Document Version
Final published version

Published in
NDT and E International

NDT and E International 107 (2019) 102126

Contents lists available at ScienceDirect

NDT and E International

journal homepage: www.elsevier.com/locate/ndteint

Diagnostic of manufacturing defects in ultrasonically welded thermoplastic composite joints using ultrasonic guided waves

Pedro Ochôa[a,b,*], Irene Fernandez Villegas[a], Roger M. Groves[b], Rinze Benedictus[a]

[a] Structural Integrity and Composites Group, Faculty of Aerospace Engineering, TU Delft, Kluyverweg 1, 2629 HS, Delft, the Netherlands
[b] Aerospace Non-Destructive Testing Laboratory, Faculty of Aerospace Engineering, TU Delft, Kluyverweg 1, 2629 HS, Delft, the Netherlands

ARTICLE INFO

Keywords:
Thermoplastic composite
Ultrasonic welding
Manufacturing defects
Structural health monitoring
Ultrasonic guided waves

ABSTRACT

This article presents research about the propagation of ultrasonic guided waves in ultrasonically welded thermoplastic composite joints. The goal of the study was to understand the effect of weld manufacturing defects on guided wave transmission across the joint. Triangular energy-directors integrated into the lower composite adherends enabled the production of defective joints in a controlled manner. The produced defect types were unwelded areas and adherend fibre bundle distortion. The reference condition corresponded to the fully welded stage which showed the highest single-lap shear strength. It was possible to detect adherend fibre bundle distortion through the increase in the negative shift of the signal characteristic frequency. Evidence of the presence of unwelded areas was found in the increase of Time-of-Flight of the maximum amplitude Lamb wave group. The sensitivity of the diagnostic parameters was found to be dependent on the ultrasonic guided wave excitation frequency.

1. Introduction

Thermoplastic composites are promising alternatives to thermoset composites in the aerospace industry owing to more cost-effective manufacturing [1]. Thermoplastic composite parts can be welded together by melting the polymeric material at their interface and consolidating the joint under pressure without risking degradation of material properties. It overcomes the typical issues of mechanical fastening of composites, such as stress concentrations and delaminations due to hole drilling, and of adhesive bonding, such as the needed surface preparation and curing cycle, and it is one of the main factors contributing to the cost-effectiveness of composite materials. There are three main techniques that are considered suitable for welding of continuous fibre reinforced thermoplastic composites: resistance, induction and ultrasonic welding [2]. Ultrasonic welding relies on the conversion of the kinetic energy of high-frequency mechanical vibrations to thermal energy at the weld interface through surface and intermolecular friction. In order to predominantly generate heat at the weld interface, thin pieces of thermoplastic polymer known as 'energy-directors' (EDs) can be placed between the parts to be welded. Once melted, the flow of the EDs promotes intimate contact and subsequently molecular interdiffusion across the overlap.

Ultrasonic welding of thermoplastic composites is an interesting technique for automation, as it requires short processing times [3]. Recent research has increased knowledge about the melting, flow and strength development mechanisms at the weld interface, enabling important advances for the application of this joining method to industrial scale. It has been shown that it is possible to use the welding process power curve and the sonotrode displacement curve to monitor and to control the ultrasonic welding process in order to obtain welds with consistent quality [3,4]. Building upon this knowledge and on previous research [5,6], Villegas et al. [7,8] studied the ultrasonic welding of thermoplastic composites with different geometries of EDs, namely loose flat film and integrated ridges with triangular cross-section, in order to understand the comparative processing advantages of both geometries. The latter ED geometry was found to enable the production of ultrasonic welds with defects (unwelded areas and adherend fibre bundle distortion) in a controlled way, which gives the opportunity to expand the structural health monitoring (SHM) capabilities for thermoplastic composite structures. In particular, it enables the study of early detection of small manufacturing defects which can affect the load bearing capability of welded joints. That research is important because, contrary to metals, it is still difficult to predict the progression of damage in composite structures [9]. This poses a serious challenge in scheduling inspection intervals and planning maintenance tasks of composite aircraft structures. And it can potentially lead to a fatal accident if unexpected failure occurs in a critical structure.

Ultrasonic guided waves (GW) are widely acknowledged to have

* Corresponding author. Structural Integrity and Composites Group, Faculty of Aerospace Engineering, TU Delft, Kluyverweg 1, 2629 HS, Delft, the Netherlands.
E-mail address: p.a.viegasochoadecarvalho@tudelft.nl (P. Ochôa).

https://doi.org/10.1016/j.ndteint.2019.102126
Received 15 October 2018; Received in revised form 13 March 2019; Accepted 2 June 2019
Available online 06 June 2019
0963-8695/

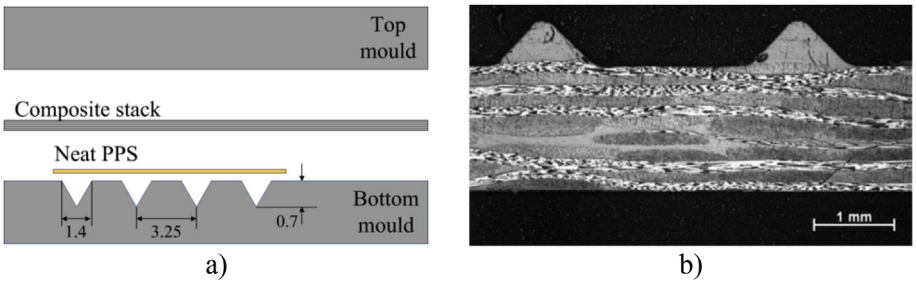

Fig. 1. a) Diagram (not to scale) with the moulds, neat PPS layers and composite stack; b) Cross-sectional micrograph of the laminate with integrated triangular EDs [8].

high potential for detailed quantitative SHM [10,11]. Over the last two decades, some studies have focused particularly on finding reliable ways of correlating changes in GW propagation with realistic defects in joints. Singher et al. [12,13] investigated the interaction of ultrasonic GW with adhesively bonded single-lap metallic joints produced with different surface treatments. Each surface treatment resulted in a different bond strength. So, to understand the effect of different surface treatment on GW propagation they used an analytical spring-mass model to describe the forces between the two adherends. As they explain, "in a quasi-static approach, the shear mechanical behaviour of the interface adhesive-adherend is represented by a density of springs with stiffness constant k" [13]. The situation of $k \rightarrow 0$ corresponds to free surfaces, while $k \rightarrow \infty$ consists of a perfect bond. And they add, "we thus attribute the parameter k, the strength of the bond". From the analytical model results, they observed a monotonic reduction of group velocity of the first symmetric GW mode with decreasing spring-stiffness constant, which is equivalent to a monotonic reduction of group velocity with decreasing bond strength. This trend was then observed experimentally, thereby confirming the validity of the model. When working in the frequency domain, Singher et al. [13] observed that the ultrasonic GW signal transmitted across the joint always had a negative shift of the characteristic frequency with respect to the ultrasonic excitation signal. They attribute "the fading of the high frequencies due to adhesive absorption" [13]. Furthermore, they also saw that this negative shift increased with decreasing bond strength. Therefore, they concluded that both group velocity and characteristic frequency shift can be used for quantifying adhesive bond strength. Kundu et al. [14] focused specifically on the detection of kissing bonds (i.e. tight physical contact between adherends without any mechanical bond). They showed that while most of the ultrasonic GW modes are insensitive to these manufacturing defects, the higher-order mode A1 is sensitive due to its non-null shear stress distributions at the bond interface within a certain range of phase velocities.

The aforementioned studies provide useful approaches on how to use ultrasonic GW to extract information about bond strength. However, none of them focused on ultrasonically welded thermoplastic composite joints. Our previous research [15] has contributed with the first known insight about the propagation of ultrasonic GW across thermoplastic composite joints welded with a flat ED of a fixed thickness. Two things were observed in the sensed GW signals acquired from the joints welded with a welding travel different from the reference travel. On the one hand, the energy transmission coefficient revealed only a small amplitude variations with respect to the reference signals. On the other hand, the correlation coefficient showed that, despite the small amplitude variations, there were large signal shape changes with respect to the reference signals. These observations were attributed to a variation in the phase velocity of the GW modes in the overlap, without a significant change of their displacement mode shapes. This affected the phase lag between the GW modes in the overlap and, consequently, the reverberation pattern inside the overlap. As a result, the modification of the interference between the reverberated wave packets and the directly transmitted wave packets was dominated by signal shape changes. A correlation between welding travel and molecular interdiffusion across the weld interface was established by benchmarking the weld interface reflection magnitude obtained through ultrasonic phased-array B-scans. Nevertheless, our previous study did not include the effect of manufacturing defects.

The research presented in this article took advantage of the utilisation of integrated triangular EDs for obtaining defective welds in a fully controlled way and study ultrasonic GW propagation through the resulting single-lap joints. The studied manufacturing defects were unwelded areas interspersed with welded zones and adherend fibre bundle distortion. Guided wave test results were analysed together with mechanical test results and optical microscopic photos of the corresponding fracture surfaces in order to understand how the changes at the weld interface affect the interaction with the guided waves. To the best of our knowledge this is the first time such a study has been conducted. By understanding how guided waves can be used to measure the weld quality we intend to establish an initial approach for diagnosing manufacturing defects in ultrasonically welded thermoplastic composite joints.

2. Methodology

2.1. Materials

Thermoplastic composite plates were manufactured from Cetex® five harness satin weave carbon fibre fabric reinforced polyphenylene sulphide (CF/PPS) semipreg material, supplied by Ten Cate Advanced Composites. Six layers were stacked according to the $[0^\circ/90^\circ]_{3s}$ sequence, where 0° and 90° correspond to the warp and weft directions, respectively. The stack was subjected to 320 °C and 10 bar for 15 min. The obtained laminates had a nominal thickness of 1.62 mm. For half of the composite stacks the lower part of the mould had triangular grooves. As shown in Fig. 1a), five 0.08 mm thick layers of neat PPS polymer were placed between the composite semipreg stack and the triangular grooves to produce consolidated plates with integrated triangular EDs [8]. It should be noted that the direction of the triangular grooves was perpendicular to the 0° direction of the composite laminate. The final height of the EDs was approximately 0.5 mm, as measured from Fig. 1b).

After manufacturing, the plates were water-jet cut into adherends with nominal dimensions of 101.6 mm × 25.4 mm (longest dimension parallel to the 0° direction of the laminate). A clamping tool (see Fig. 2) was used to ensure the overlap had a nominal length of 12.7 mm (according to standard ASTM D1002 [16]), while preventing undesirable movement of the samples during the ultrasonic welding process. Nevertheless, the adherends still had to be manually sanded along the longitudinal edges in order to tightly fit the tool. As explained later in subsubsection 4.3.1, it is important to highlight that the bottom mould had been originally produced for other research projects, with two sets of four triangular grooves. Because of that an additional sanding operation had to be performed in order to have only one set of four ED rows and to allow the adherends to fit inside the clamping tool.

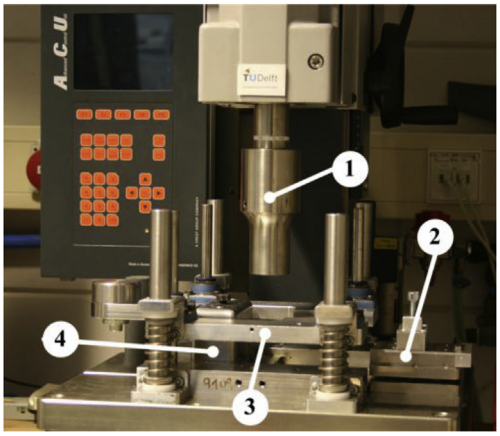

Fig. 2. Ultrasonic welding setup: 1) sonotrode, 2) top clamp, 3) sliding frame for top clamp, 4) bottom clamp.

2.2. Batch and test matrix definition

For the production of the specimens with weld defined qualities we needed to consider the previous knowledge about the evolution of the welding process power and the sonotrode displacement (from here onwards called travel) with integrated triangular EDs, as studied by Villegas and Palardy [8]. In order to be consistent with the welding conditions employed by them the same force, amplitude and solidification parameters were used: 500 N welding force, 86.2 µm peak-to-peak vibration amplitude, 1000 N solidification force, and 4 s solidification time. It was decided to produce three batches of specimens. An initial weld was produced with a travel of 0.5 mm in order to extract the power and travel curves covering all the process stages, shown in Fig. 3.

Based on those curves, the process parameters for the different weld stages were selected. The welding process parameters used for the three batches and the corresponding specimen names are summarised in Table 1. Specimens were named according to the convention B {batch#}-{specimen#}. Batch 1 was produced by stopping the travel-controlled process at the start of the travel plateau (see first vertical line in Fig. 3), with a value of 0.36 mm. At that point the welds are expected to be incomplete, with interspersed welded and unwelded areas [8]. That state is reached after melting, collapse and partial flow of the EDs into the gaps between the adherends, where the melt-fronts are arrested by coming into contact with the adjacent colder adherends (see Fig. 4A–C) [8]. Batch 2 was produced by stopping the process at the end of the travel plateau (see second vertical line in Fig. 3). Since the transition from the first to the second welding point occurs at the same travel, it was decided to use energy-control welding, with a value of E = 550 J. At this point the joint is expected to be fully welded, after the previously arrested ED melt-fronts are remelted and start to flow out of the overlap (see Fig. 4 D) [8]. Finally batch 3 was produced by taking the travel-controlled process beyond the power peak (see third vertical line in Fig. 3). At this weld stage EDs are expected to be completely squeezed out from the welding interface, with melt and flow of the matrix beyond the first layer of the adherends (see Fig. 4 E) [8], which is expected to lead to adherend fibre bundle distortion [3].

Table 1
Welding process control parameters for the three batches and corresponding specimen names.

Specimen group	Control parameter	# Joints	Specimen names
Batch 1	Travel: 0.36 mm	5	B01-01 to B01-05
Batch 2	Energy: 550 J	5	B02-01 to B02-05
Batch 3	Travel: 0.42 mm (× 1); 0.44 mm (× 3)	4	B03-01 to B03-04

3. Experiments

3.1. Ultrasonic guided wave testing

The full GW testing setup is shown in Fig. 5. The ultrasonic excitation was produced by an Agilent 33500 B arbitrary waveform generator and transmitted to the specimen by a piezo-ceramic (PZT) transducer. The same type of PZT transducer was used to sense the ultrasonic response which was then acquired by a PicoScope 6402 A digital oscilloscope. The raw ultrasonic signals can be found in Ref. [17].

The excitation signal shape and frequency, and the PZT transducers geometry were selected based on a design methodology [18] which optimises the sensor output, the coupled electro-mechanical response of the transducer-structure assembly, the energy transfer from the bonded PZT transducer to the structure, the available area for transducer bonding, and the measurement equipment capabilities. As a result, the PZT transducers consisted of bare APC 850 material (provided by American Piezo Ltd) cut into discs of 10 mm diameter and 0.4 mm thickness, and poled in the out-of-plane direction. They were bonded to the composite adherends at the positions indicated in Fig. 6. The excitation signal was a sinusoidal tone-burst with a 10-cycle Hanning window amplitude modulation generated at four frequencies: 204, 349, 486 and 619 kHz. At 204 and 349 kHz, the maximum input voltage was around 9 V, and the maximum output voltage was between 250 and 460 mV. At 486 and 619 kHz, the maximum input voltage was around 8 V, and the maximum output voltage was between 23 and 37 mV. According to the dispersion curves in Fig. 7, at these frequencies the GW modes expected in the adherends are up to order one, while in the overlap the expected GW modes are up to order two. By testing at multiple frequencies it was possible to explore the sensitivity of both zero- and higher-order GW modes to the different welding defects.

3.2. Complementary testing and evaluation

The welded joints were mechanically tested according to the ASTM D1002 standard in a Zwick/Roell 250 kN testing machine, in order to extract the single-lap shear strength (SLSS). The resulting fracture surfaces were photographed with a Zeiss SteREO Discovery.V8 microscope. The SLSS results and the fracture surface observations were used 1) to define the reference batch, and 2) to check if the joints had been welded with the manufacturing defects desired for this research.

4. Results and discussion

4.1. Selection of the reference state

The maximum load carried by the specimens during the single-lap shear tests was divided by the total overlap area to obtain the apparent

Fig. 3. Power and travel curves as function of energy for the initial weld, produced with a travel 0.5 mm. These curves were used to select the process parameters for the three batches. The welding points for the three batches are indicated by vertical dashed lines.

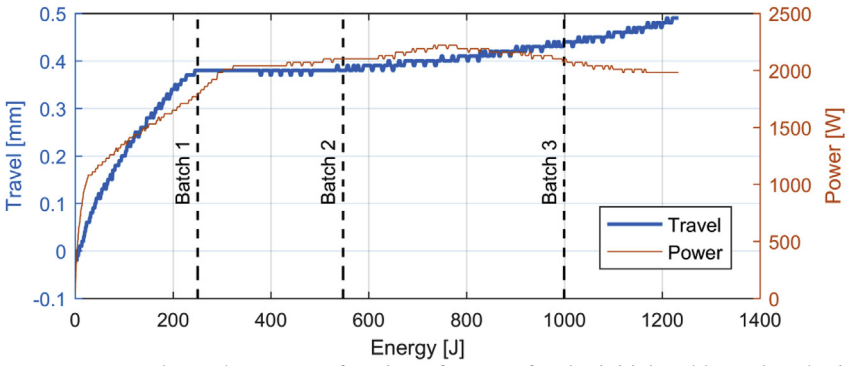

Fig. 4. Different phases of the ultrasonic welding process with triangular EDs: A) intact EDs; B) collapse of EDs due to melting; C) partial flow of the EDs and melt-front arrest; D) remelting of ED melt-fronts and subsequent flow out of the overlap; E) complete ED squeeze out from the welding interface, with melt and partial flow of the matrix beyond the first adherend layer.

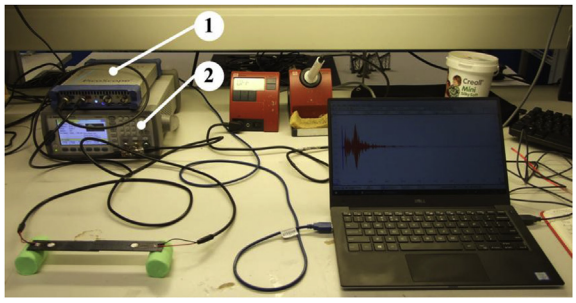

Fig. 5. Complete set-up used for ultrasonic guided wave testing: 1) digital oscilloscope; 2) waveform generator.

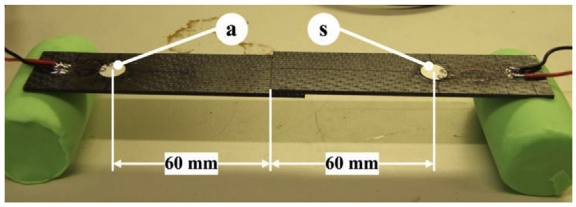

Fig. 6. Single-lap joint instrumented with piezo-ceramic transducer discs, one functioning as actuator (a) and the other as sensor (s).

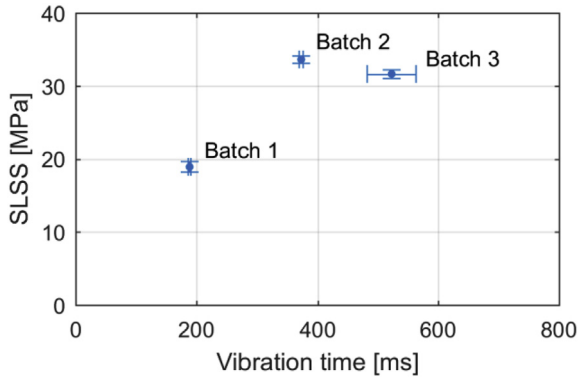

Fig. 8. Single-lap shear strength as a function of welding vibration time.

SLSS. The results are plotted in Fig. 8. The single-lap shear tests were useful to define the reference state for this study. Since, the maximum SLSS was achieved for batch 2 and the fracture surfaces of batch 2 specimens (see Fig. 9) indicate a uniform welding quality without any unmolten EDs or fibre bundle distortion, it was decided to designate it as the reference one.

4.2. Evaluation of process consistency

The purpose of this section is to display proof that the desired

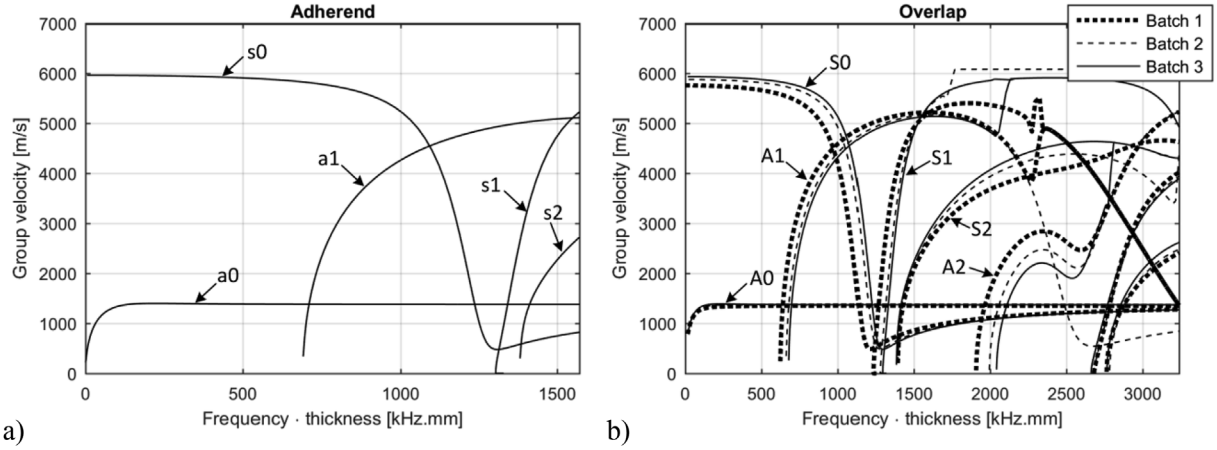

Fig. 7. Simulated group velocity curves for a) the adherends and b) the overlaps of the three batches. The curves were computed with the DISPERSE™ software (Imperial College, London) using the approximations explained in Ref. [15]. The curves provide an approximation of the dispersive properties of the guided wave modes in the structures tested in this study. The joints were modelled as inifinite layered constructions composed by two 1.62 mm thick CF/PPS plates (with elastic properties according to Daggumati et al. [19]) and one fully connected layer in between representing the weld-line. The weld-line for each batch was modelled as a layer of isotropic material with the elastic properties of neat PPS resin [20] and a thickness approximately equal to the remaining amount of material between the two adherends: 0.29 mm for batch 1, 0.12 mm for batch 2, and 0.04 mm for batch 3. DISPERSE™ does not allow the simulation of the welding defects analysed in this study (unwelded areas and adherend fibre distortion), nor does it allow molecular interdiffusion between the weld-line and the adherends to be taken into account.

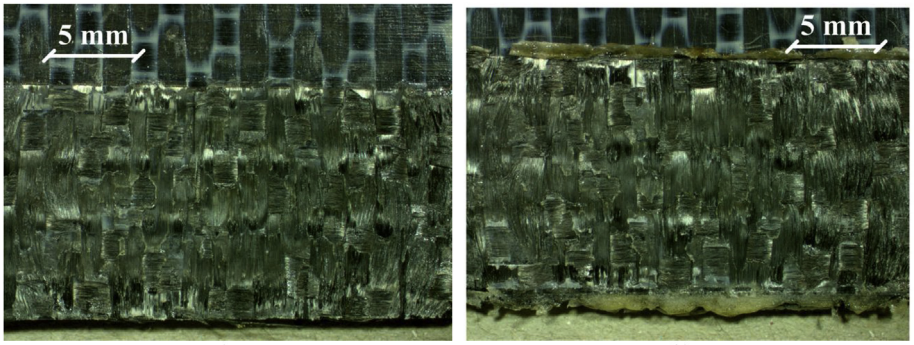

Fig. 9. Fracture surfaces of the a) bottom and b) top adherends of specimen B02-02 (batch 2).

manufacturing defects were effectively introduced in a fully controlled way during the ultrasonic welding process.

4.2.1. Batch 1

There were portions of the EDs that did not melt entirely and/or had resolidified before full molecular interdiffusion could be established across the areas through which they had flowed (see Fig. 4 in subsection 2.2). This was confirmed by the presence of remnant EDs on the bottom adherent after failure (Fig. 10a) and by the welded areas interspersed with unwelded areas on the top adherent after failure (Fig. 10b).

4.2.2. Batch 3

When comparing the fracture surfaces of batch 1 in Fig. 9 with those of batch 3 in Fig. 11 it is possible to confirm that the fibre bundles are no longer entirely perpendicular to each other, as they are deformed in directions which are slightly concentric with respect to the middle point of the facture surface.

4.3. Ultrasonic guided wave detection

This article builds upon our previous study of GW transmission across ultrasonically welded thermoplastic composite joints [15]. For a matter of consistency with that work, the GW signals are analysed in the time and frequency domains by exploring the same parameters of signal energy, characteristic frequency, wave group Time-of-flight, and correlation coefficient.

4.3.1. Signal energy

The energy, *Es*, of the time-domain GW signal, *x(t)*, was defined as [21,22].

$$Es = \int_{t_i}^{t_f} |x(t)|^2 dt \tag{1}$$

where t_i and t_f, are the initial and final recorded time instants. For all the excitation frequencies the average time-domain GW signal energy for the three batches is plotted in Fig. 12.

The high standard deviation of the mean values makes it very difficult to establish a clear logical trend. This large data scatter seems to be related to intra-batch variability. As explained in subsection 2.1, during the preparation of the adherends it was necessary to sand them twice. First to remove the extra set of ED rows. This created adherend thickness variability, as illustrated in Fig. 13a). Second to trim the adherends width so that they would fit in the welding fixture. This added extra dimensional variability, as shown in Fig. 13b). These two sanding operations created dimensional and mass variability among specimens of the same batch. As a result there was variability in final overlap thicknesses in each batch, as plotted in Fig. 14.

As we have previously shown [15], small variations of weld line thickness (resulting in small variations of final overlap thickness) determine the possible overlap GW modes and influence their compatibility with the adherend GW modes, thereby determining the amount of ultrasonic energy transmitted across the welded joint. As we have seen above, intra-batch adherend dimensional variability led to joints with different final overlap thicknesses. This means each specimen was in fact tested at a different 'frequency × thickness' point of the dispersion curves (see Fig. 7), even though the excitation frequency was the same. Consequently, the possible adherend and overlap guided wave modes and their compatibility were different for each specimen, and so was the received signal energy. The effect of that variability is strongly felt in the GW signal energy results because the number of overlap modes is large and their characteristics vary sharply with frequency, as depicted in Fig. 7b).

Nevertheless, Fig. 12 clearly shows that at 486 kHz the energy for batch 1 is lower than for batch 2, which is in agreement with the expected results. The weld interface of batch 1 is thicker and still has some unwelded regions, consisting of a larger acoustic impedance mismatch than in the case of batch 2, and thereby transmitting less energy than in the case of batch 2.

The lack of a clear trend in the energy results makes it impossible to use them for indicating the presence of the different manufacturing defects. However, they constitute strong evidence that tenuous intra-

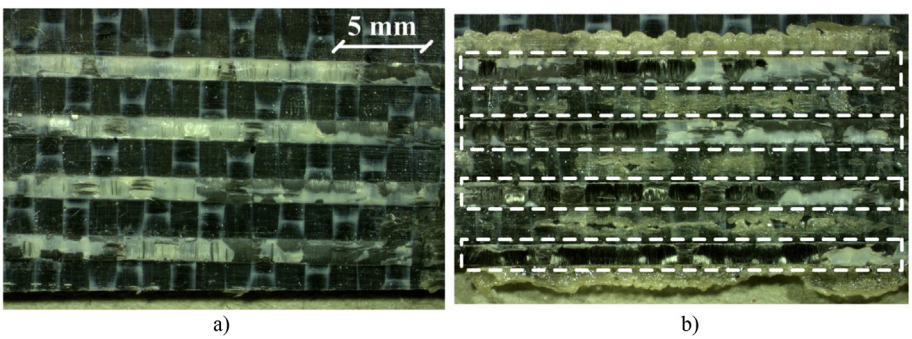

Fig. 10. Fracture surfaces of the a) bottom and b) top adherends of specimen B01-04 (batch 1), welded with travel equal to 0.36 mm. In a) it is possible to see rows of whitish remnant EDs. In b) it is possible to see welded areas (highlighted by dashed-line rectangles) interspersed with unwelded areas (zones between the dashed-line rectangles). Also in b) irregular flow fronts in the unwelded areas indicate melt, incomplete squeeze-out and resolidification of the EDs.

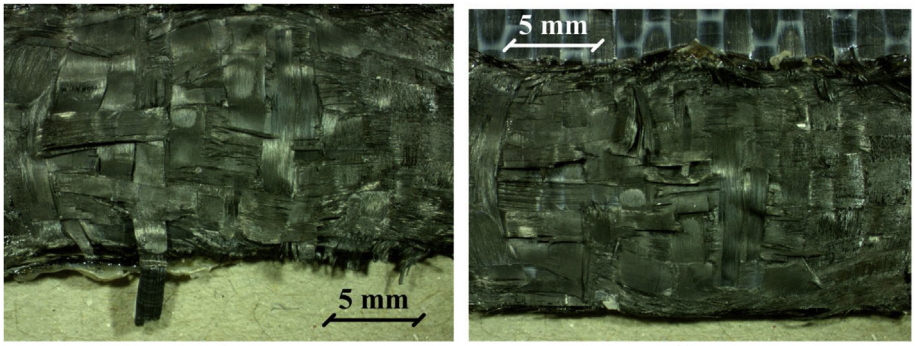

Fig. 11. Fracture surfaces of the a) bottom and b) top adherends of specimen B03-02 (batch 3).

batch variability has a relevant impact on the GW test signals, despite the SLSS results showing adequate process consistency.

4.3.2. Characteristic frequency

According to Singher [13], the spectrum of the excited ultrasonic guided wave signal is always shifted towards the lower frequencies after passing through an adhesive bond. That negative shift increases when there is a delamination or a disbond. So it is possible to infer the bond strength by extracting the characteristic frequency shift (Δf_{ch}). For this study it was decided to assess the sensitivity of this signal feature to manufacturing defects in the ultrasonic weld, with a special focus on adherend fibre bundle distortion. To that end, the following hypothesis was formulated. As it is known from theory, the propagation of ultrasonic GW in composites follows the anisotropy of the material, i.e. they propagate preferentially along the directions with the highest stiffness, which in turn depend on the directions of the fibres. If the ultrasonic GW were scattered sideways by the distorted fibre bundles of the adherends, then the GW would be transmitted across the joint in more oblique directions which in turn would originate more reflections from the edges. These reflections would then be superimposed, thereby adding more side-frequencies to the signal. This would induce a more spread frequency spectrum and a larger negative shift of the characteristic frequency.

As in Ref. [13], the characteristic frequency (f_{ch}) was computed according to

$$f_{ch} = \sum_{i=1}^{i=n} FFT(x)_i \cdot f_i \Big/ \sum_{i=1}^{i=n} FFT(x)_i \tag{2}$$

which corresponds to the average of all f_i frequencies in the fast-Fourier-transformed (FFT) signal (with points from $i = 1$ to $i = n$) weighted by the corresponding FFT coefficients. The shift Δf_{ch} was then calculated as the characteristic frequency difference between the sensed signal and the excitation. The results for each batch, at each frequency are presented in Fig. 15.

At 204 kHz there is almost no shift for any of the batches, with Δf_{ch} ranging between 2 kHz for batch 1 and 0.5 kHz for batch 3. At that frequency the only overlap GW mode shape which has a non-null in-plane component at the weld interface is the S0, as shown in Fig. 16a). It has a wavelength of around 30 mm, which is larger than the overlap thickness and overlap length, and thus the weld line does not seem to have the negative shifting effect on f_{ch} [13]. At 349 kHz there is a negative Δf_{ch} of about −20 kHz, meaning there is an in-plane interaction with the weld line. Since the S0 mode is still the only overlap GW mode shape with a non-null in-plane component at the weld interface, the Δf_{ch} value can be attributed to the wavelength of the S0 mode being approximately equal to the overlap length. However, this same fact prevents the detection of discontinuities within the overlap length by the S0 mode. In other words, the interaction is still not detailed enough to enable the differentiation between batches.

At 486 and 619 kHz, there is a more pronounced negative Δf_{ch} for all batches, together with an increase in standard error, meaning that the interaction with the weld interface is stronger than at 204 and 349 kHz. This is caused by an increase in the number of overlap GW mode shapes with non-null in-plane component at the weld interface from one to three: S0, S1 and S2 (see Fig. 16b). Nevertheless, the scatter shown for batch 3 at 486 kHz prevents clear conclusions about the differences between batches 2 and 3. This scatter is probably due to the fact that only the S0 wavelength (around 4 mm) is smaller than the overlap length, while the S1 and S2 wavelengths are larger (around 13 and 28 mm, respectively), therefore still hindering a detailed interaction with the weld interface for all measurements of batch 3. But at 619 kHz, we observe that while Δf_{ch} is almost constant for batches 1 and 2, there is a clear increase in negative Δf_{ch} from batch 2 to batch 3, which can only indicate the presence of adherend fibre bundle distortion. It is possible to verify that the spatial resolution of the interaction with the weld interface was increased because both S0 and S1 wavelengths are both smaller than the overlap length (around 3 and 10 mm, respectively), and only the S2 wavelength remains larger than the overlap length. Therefore, the results for 619 kHz corroborate our hypothesis. Although it was not possible to detect the unwelded areas, the

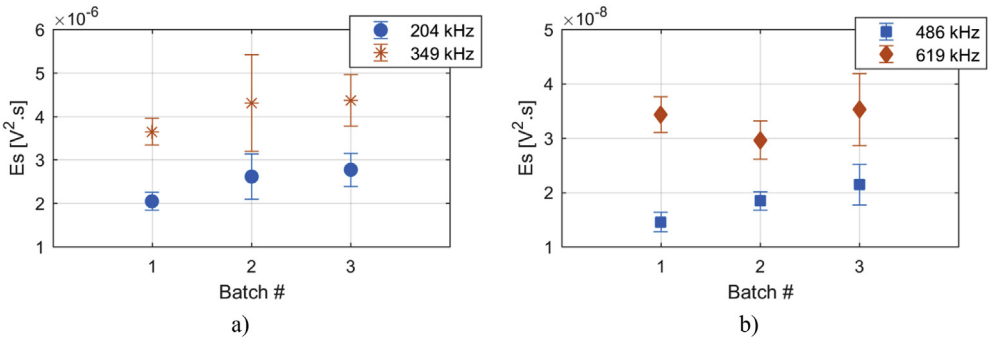

Fig. 12. Time-domain signal energy for each batch at all excitation frequencies.

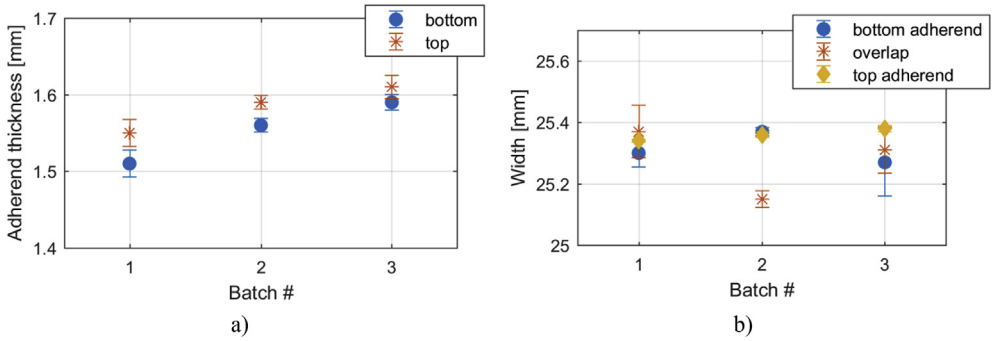

Fig. 13. a) Variation of adherend thickness per batch; b) Variation of width in the three main zones of the single-lap joint specimens for each batch.

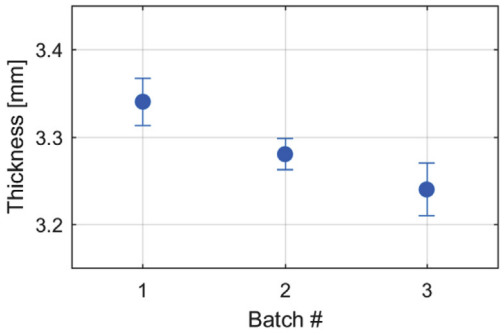

Fig. 14. Overlap thickness for each batch.

characteristic frequency shift appears to be a suitable parameter to indicate the presence of adherend fibre bundle distortion, as long as there are multiple overlap GW mode shapes with non-null in-plane component at the weld interface and with wavelengths smaller than the overlap length.

4.3.3. *Time-of-Flight*

When considering ultrasonic GW propagation in composite materials, particle motion along one direction can induce motion in the perpendicular one, because the fibre direction changes across the thickness of the laminate. Consequently, all GW modes are coupled, some of them with very similar group velocities, as in the case of the S0 mode and the SH0 mode. This makes it almost impossible to identify the different GW modes, and to correlate their changes to interactions with different damage types [23]. Additionally, as introduced in Section 1, group velocity has been shown to be positively correlated to the bond strength of joints [12,13]. The group velocity is inversely proportional to the Time-of-Flight (ToF), i.e. the time a certain wave group takes to propagate along a certain known distance. Taking these two aspects into account, the definition of ToF was adapted in order to avoid incorrect conclusions. In our experiment, ToF was taken as the time interval between the maximum amplitude point of the excitation pulse and the maximum amplitude point of the sensed signal. This definition allows a direct correspondence between ToF and group velocity to be established, without requiring a direct calculation of the group velocity of any specific GW mode. The point of maximum amplitude of the sensed signal may correspond to the maximum amplitude point of a directly arriving GW mode, but it may also be the result of constructive interference between a direct arrival and a reverberation, or between a direct arrival and a reflection, or both. Nevertheless, any difference in the time at which that maximum amplitude point occurs at a specific frequency can be attributed to a change in the group velocity of one or more GW modes. Therefore, by capturing differences in TOF defined in this way, it is possible to indirectly assess changes in group velocity. The results for the three batches at each excitation frequency are plotted in Fig. 17.

As with the signal energy results, there is considerable variability within batches. However, in the cases of 204 and 619 kHz it is possible to identify a clear drop from batch 1 to batch 2 of about 29 and 48 μs, respectively. The fact that a clear ToF drop from batches 1 to 2 was consistently found at 204 and 619 kHz appears to correlate well with the magnitude of the changes occurring at the weld interface in the transition from batch 1 to batch 2 conditions. While the thickness variation from batch 1 to batch 2 was approximately the same as from batch 2 to batch 3 (see Fig. 14), the joint had the most pronounced variation from batches 1 to 2, as it is in this transition that the joint becomes fully welded and the weld line continuous. This transformation had a marked effect on the single-lap shear strength, with batch 1 specimens consistently having a substantially lower failure load than those of batch 2 specimens, as seen in Fig. 18 (see the average SLSS values for each batch in Fig. 8). Therefore, corroborating the proportionality of ToF to weld strength. It is important to note that the ToF drop at 204 kHz is three orders of magnitude higher than the values found in our previous study [15] for the maximum ToF difference caused only by differences in weld line thickness at the same excitation frequency.

Also in Fig. 17b), for batch 2 at 619 kHz, it is possible to clearly identify a global minimum at the frequency. From batch 2 to batch 3,

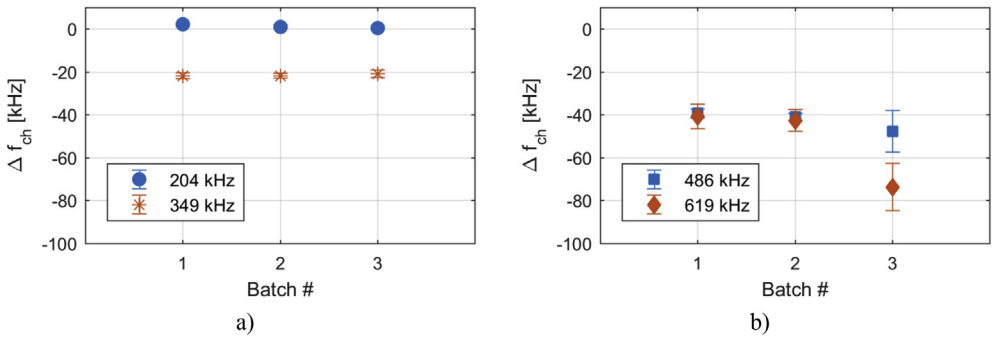

Fig. 15. Characteristic frequency shift for the three batches at all excitation frequencies.

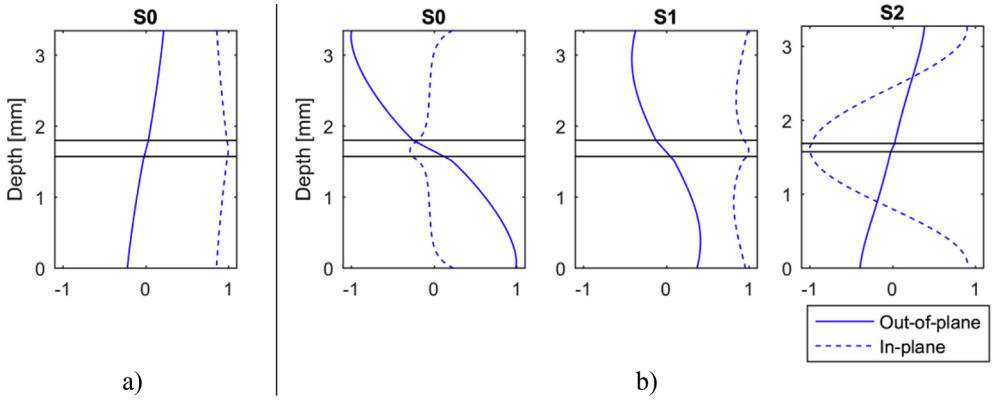

Fig. 16. Guided wave displacement mode shapes with non-null in-plane component at the weld interface, for batch 3 overlaps, typically occurring at a) 204 and 349 kHz, and b) 486 and 619 kHz. The mode shapes were extracted by using the "Mode Shapes" tool of DISPERSE™ after tracing the dispersion curves in Fig. 7.

the molecular interdiffusion and the crystallographic structure of the weld line are almost unaltered, and the main change is the distortion of adherend fibre bundles (as visible from the comparison of Fig. 9 in subsection 4.1 and Fig. 11 in subsubsection 4.2.2), with no visible effect on the load-displacement curve slope (see Fig. 18). As shown in subsubsection 4.3.2 the strongest and most detailed interaction of the GW with the weld interface occurs at 619 kHz, with the distorted fibre bundles of the adherends scattering the waves sideways and inducing extra reflections from the overlap edges. The occurrence of these extra reflections can clearly be identified by the larger number of narrow wave packets in the signals of batch 3 when compared to signals from batch 2, as shown in Fig. 19. These reflections arrive at time instants very close to each other and interfere constructively, generating a wave packet with maximum amplitude at a later time than for batch 2. As a consequence, the ultrasonic energy arrives at the sensor at a slower rate for batch 3 than for batch 2, as illustrated by the corresponding average normalised cumulative energy curves in Fig. 20.

Given the results presented here, it seems that ToF is sensitive to both unwelded areas interspersed with welded zones and adherend fibre bundle distortion. Nevertheless, if Δf_{ch} and ToF are analysed together, it is possible to distinguish these two defective scenarios:

a) Null Δf_{ch} and high ΔToF → Unwelded areas interspersed with welded zones
b) High Δf_{ch} and high ΔToF → Adherend fibre bundle distortion

This detection criterion requires the definition of low-high thresholds for Δf_{ch} and ΔTOF. For Δf_{ch} the threshold is set at −20 kHz, based on the lowest non-null average values observed among all tested frequencies (see Fig. 15a). For ΔTOF the threshold is set at 28 μs, based on the minimum average TOF difference that allows a distinction between batch 1 and 2 at 204 kHz (see Fig. 17a). Using these thresholds, the obtained detection accuracy for unwelded areas is around 60% at 204 kHz, while the detection accuracy for adherend fibre bundle distortion is around 100%.

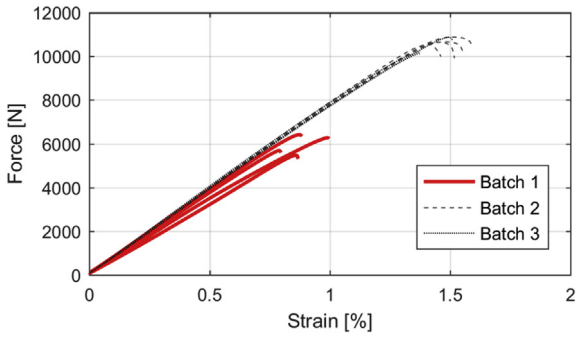

Fig. 18. Force-displacement curves from single-lap shear tests.

4.3.4. *Correlation coefficient*

As in our previous study [15], it was decided to resort to the correlation coefficient (CC) in order to quantify signal shape variations. The CC was computed between each batch 2 specimen and each specimen of the other batches for each frequency. The CC was first computed between full time-domain signals, i.e. without excluding any information about signal amplitude or phase. It was decided to take the complement of the CC (CCcomp = 1 - CC) in order to make it a direct indicator of the differences between signals, i.e. the higher CCcomp, the larger the difference. The results are plotted in Fig. 21.

It is possible to see that at 204 and 349 kHz the CCcomp values for both batches are grouped between 0.3 and 0.6, while at 486 and 619 kHz, they are grouped between 0.7 and 0.9, without a clear difference in level between batch 1 and batch 3. Despite the relatively large scatter, one could argue that at 486 and 619 kHz there were more GW signal changes than at 204 and 349 kHz. However, when phase

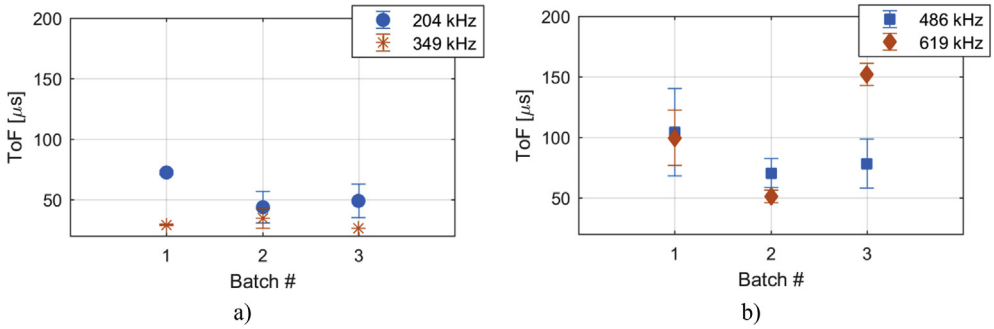

Fig. 17. Time-of-Flight for the three batches at all excitation frequencies.

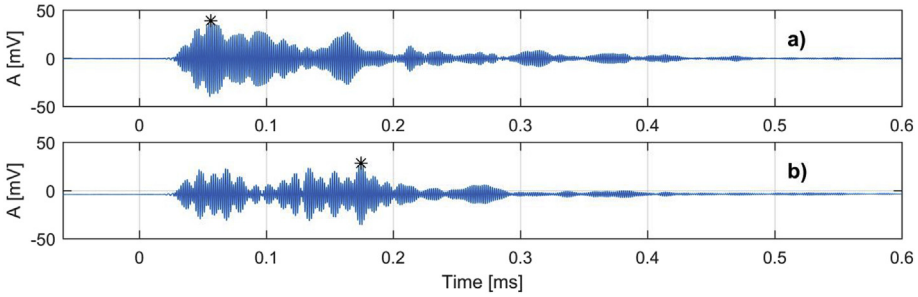

Fig. 19. Ultrasonic GW signals from a) batch 2 (specimen B02-04) and b) batch 3 (specimen B03-04). The point of maximum amplitude in indicated with an asterisk.

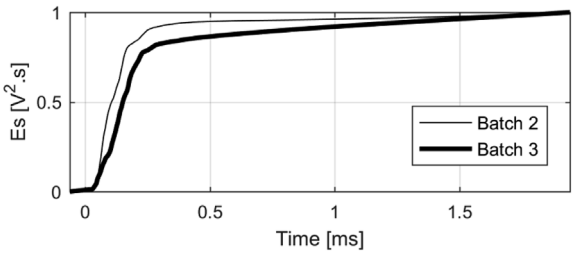

Fig. 20. Average normalised cumulative energy curves for batch 2 and batch 3.

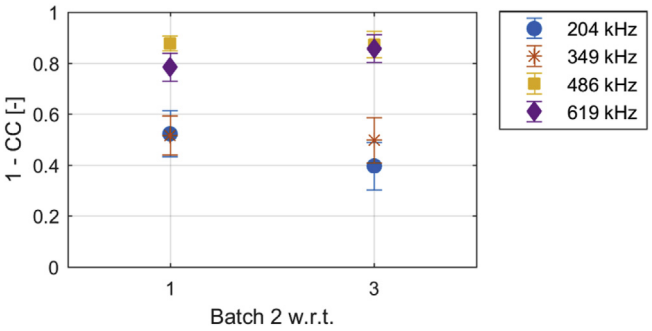

Fig. 21. Complement of the correlation coefficient (1 - CC) between full time-domain signals from batch 2 and the other batches for each excitation frequency.

information is excluded and the CCcomp is computed between the time-domain signal envelopes (see Fig. 22a), all the obtained values seem to cluster between 0.1 and 0.3, with much lower standard error than in the case of the full time-domain signal. This shows that most of the GW signal shape changes are due to phase variations. In fact, the lower standard errors show that the consequences of intra-batch variability in ultrasonic GW metrics are mainly due to signal phase differences. This is in agreement with the conclusion from our previous research [15] that transformations at the weld interface affect ultrasonic GW propagation mainly by causing differences in reverberation pattern, and in the interference between reverberations and directly arriving groups.

The CCcomp was also computed for the frequency-domain signals (see Fig. 22b), in which phase information is also not taken into account. The results fall approximately in the same range as those in Fig. 22a). However, there is a larger separation between 204/349 kHz and 486/619 kHz for batch 3, than in Fig. 22a). This seems to be in agreement with our observations from subsubsection 4.3.2 that the frequency spectrum of the signal is more affected by adherend fibre bundle distortion than by unwelded areas.

5. Conclusions

This article presented research about the propagation of ultrasonic guided waves (GW) in ultrasonically welded thermoplastic composite joints. The goal of the study was to understand the effect of weld manufacturing defects on GW transmission across the joint.

Triangular energy-directors integrated into the lower composite adherends enabled the production of defective joints in a controlled manner. The produced defect types were unwelded areas interspersed with welded zones (batch 1), and adherend fibre bundle distortion due to overwelding (batch 3). The reference condition (batch 2) corresponded to the fully welded stage in between the other two, which showed the highest single-lap shear strength. Ultrasonic GW tests were performed at four frequencies (204, 349, 486 and 619 kHz). Excitation and sensing were accomplished by thin piezo-ceramic discs installed on the adherends at opposite sides of the overlap.

The negative shift of the characteristic frequency (Δf_{ch}) showed a consistent increase with excitation frequency, revealing an increasing strength of the interaction of the ultrasonic GW with the weld interface. At 619 kHz, the interaction was strong and detailed enough to allow the distinction between batch 2 and batch 3. The significant increase in negative Δf_{ch} is attributed to the oblique scattering effect of the distorted fibre bundles on the GW. Thus, although it was not possible to detect the unwelded areas, the characteristic frequency shift appears to be a suitable parameter to indicate the presence of adherend fibre bundle distortion.

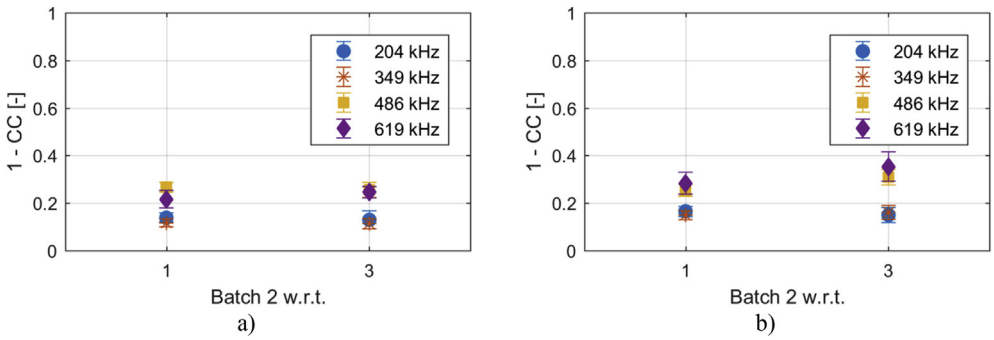

Fig. 22. Complement of the correlation coefficient (1 - CC) between batch 2 and the other batches for each excitation frequency for a) the time-domain signal envelopes, and b) for the frequency-domain signals.

At 204 and 619 kHz, the lowest Time-of-Flight (ToF) was consistently found for the reference batch. The batch 1 joints had a significantly higher ToF than the reference specimens, meaning the wave group of maximum energy was slower for that defective case than for the reference one. Given the known sensitivity of ToF to joint stiffness changes, the results were considered to be well correlated with the lower failure load of the single-lap tests performed on batch 1 joints. Also at 619 kHz, batch 3 was found to have the highest ToF of all. This was due to the oblique scattering effect of the distorted fibre bundles on the GW, which caused the extra reflections from the overlap edges to interfere constructively and form the wave packet of maximum amplitude at a late time instant. Therefore it was concluded that ToF is sensitive to both unwelded areas interspersed welded zones and adherend fibre bundle distortion.

The analysis of the correlation coefficient (CC), computed between each batch 2 specimen and each specimen of the other batches for each frequency, added extra confidence to the conclusion that the frequency spectrum of the signal is more affected by adherend fibre bundle distortion than by unwelded areas.

In summary, by combining Δf_{ch} and ToF analysis it was possible to detect and distinguish the two defective scenarios. The case of null Δf_{ch} and high ΔToF with respect to the reference corresponded to unwelded areas interspersed with welded zones, with a detection accuracy around 60%. The case of high Δf_{ch} and high ΔToF with respect to the reference corresponded to adherend fibre bundle distortion, with a detection accuracy of 100%.

To the best of our knowledge this is the first time such a study has been conducted. By understanding how ultrasonic GW interact with the weld interface at different weld stages, it is intended to establish an initial approach for diagnosing manufacturing defects in ultrasonically welded thermoplastic composite joints. In turn this is an important step towards the development of structural health monitoring capabilities for modern thermoplastic composite aircraft structures, where early detection of incipient defects is crucial to prevent unexpected failures.

Data availability

The raw data required to reproduce these findings are available to download from 10.4121/uuid:190ac321-ad31-456c-919e-564f7e6333ef. The processed data required to reproduce these findings are available to download from 10.4121/uuid:190ac321-ad31-456c-919e-564f7e6333ef.

Acknowledgements

This research is part of the Thermoplastic Affordable Primary Aircraft Structure 2 (TAPAS 2) project, financed by the Netherlands Enterprise Agency of the Ministry of Economic Affairs.

References

[1] Red C. The outlook for thermoplastics in aerospace composites, 2014-2023. High Perform Composite Sep 2014;22(5):54–63.
[2] Villegas IF, Moser L, Yousefpour A, Mitschang P, Bersee HEN. Process and performance evaluation of ultrasonic, induction and resistance welding of advanced thermoplastic composites. J Thermoplast Compos 2012;26(8):1007–24.
[3] Villegas IF. In situ monitoring of ultrasonic welding of thermoplastic composites through power and displacement data. J Thermoplast Compos 2015;28(1):66–85.
[4] Villegas IF. Strength development versus process data in ultrasonic welding of thermoplastic composites with flat energy directors and its application to the definition of optimum processing parameters. Compos Part A - Appl S 2014;65:27–37.
[5] Tateshi N, North TH, Woodhams RT. Ultrasonic welding using tie-layer materials. Part I: analysis of process operation. Polym Eng Sci 1992;32:600–11.
[6] Yan J, Wang X, Li R, Xu H, Yang S. The effects of energy director shape on temperature field during ultrasonic welding of thermoplastic composites. Key Eng Mater 2007;353–358:2007–10.
[7] Villegas IF, Valle Grande B, Bersee HEN, Benedictus R. A comparative evaluation between flat and traditional energy directors for ultrasonic welding of CF/PPS thermoplastic composites. Compos Interfac 2015;22(8):717–29.
[8] Villegas IF, Palardy G. Ultrasonic welding of CF/PPS composites with integrated triangular energy directors: melting, flow and weld strength development. Compos Interfac 2017;24(5):515–28.
[9] Kassapoglou C. Design and analysis of composite structures: with applications to aerospace structures. second ed. Wiley; 2013.
[10] Su Z, Ye L, Lu Y. Guided Lamb waves for identification of damage in composite structure: a review. J Sound Vib 2006;295:753–80.
[11] Mitra M, Gopalakrishnan S. Guided wave based structural health monitoring: a review. Smart Mater Struct 2016;25(053001):1–27.
[12] Singher L, Segal Y, Segal E. Considerations in bond strength evaluation by ultrasonic guided waves. J Acoust Soc Am 1994;96(4):2497–505.
[13] Singher L. Bond strength measurement by ultrasonic guided waves. Ultrasonics 1997;35:305–15.
[14] Kundu T, Maji A, Ghosh T, Maslov K. Detection of kissing bonds by Lamb waves. Ultrasonics 1998;35:573–80.
[15] Ochôa P, Villegas IF, Groves RM, Benedictus R. Experimental assessment of the influence of welding process parameters on Lamb wave transmission across ultrasonically welded thermoplastic composite joints. Mech Syst Signal Process 2018;99:197–218.
[16] ASTM D1002-10. Standard test method for apparent shear strength of single-lap-joint adhesively bonded metal specimens by tension loading (Metal-to-Metal). 2010.
[17] Viegas Ochôa de Carvalho PA. Supporting data for Ultrasonic guided wave and single-lap shear tests in defective ultrasonically welded thermoplastic composite joints. 4TU.Centre for Research Data; 2019. Dataset https://doi.org/10.4121/uuid:190ac321-ad31-456c-919e-564f7e6333ef.
[18] Ochôa P, Groves RM, Benedictus R. Systematic multi-parameter design methodology for an ultrasonic health monitoring system for full-scale composite aircraft primary structures. Struct Contr Health Monit 2019:e2340.
[19] Daggumati S, De Baere I, Van Paepegem W, Degrieck J, Xu J, Lomov SV, Verpoest I. Local damage in a 5-harness satin weave composite under static tension: part II – Meso-FE modelling. Compos Sci Technol 2010;70:1934–41.
[20] TenCate Cetex TC1100 PPS Resin System, TenCate advanced composites, product datasheet revised 05-2014.
[21] Smith SW. Digital signal processing: a practical guide for engineers and scientists. second ed. USA: Newness – Elsevier Science; 2003.
[22] Boashash Boualem, editor. Time frequency signal analysis and processing: a comprehensive reference. Elsevier Ltd.; 2003.
[23] Putkis O, Dalton RP, Croxford AJ. The anisotropic propagation of ultrasonic guided waves in composite materials and implications for practical applications. Ultrasonics 2016;65:390–9.